

Real-time four-dimensional scanning transmission electron microscopy through sparse sampling

A W Robinson, J Wells, A Moshtaghpour, D Nicholls, C Huang, A Velazco-Torrejon, G Nicotra, A I Kirkland, and N D Browning

Citation: Chin. Phys. B, 2024, 33 (**11**): 116804. DOI: 10.1088/1674-1056/ad8a4a
Journal homepage: http://cpb.iphy.ac.cn; http://iopscience.iop.org/cpb

What follows is a list of articles you may be interested in

Multidimensional images and aberrations in STEM

Eric R. Hoglund and Andrew R. Lupini
Chin. Phys. B, 2024, 33 (**9**): 096807. DOI: 10.1088/1674-1056/ad73b2

Atomically self-healing of structural defects in monolayer WSe_2

Kangshu Li(李康舒), Junxian Li(李俊贤), Xiaocang Han(韩小藏), Wu Zhou(周武), and Xiaoxu Zhao(赵晓续)
Chin. Phys. B, 2024, 33 (**9**): 096804. DOI: 10.1088/1674-1056/ad641f

Revealing the microstructures of metal halide perovskite thin films via advanced transmission electron microscopy

Yeming Xian(冼业铭), Xiaoming Wang(王晓明), and Yanfa Yan(鄢炎发)
Chin. Phys. B, 2024, 33 (**9**): 096803. DOI: 10.1088/1674-1056/ad6259

Symmetry quantification and segmentation in STEM imaging through Zernike moments

Jiadong Dan, Cheng Zhang, Xiaoxu Zhao(赵晓续), and N. Duane Loh
Chin. Phys. B, 2024, 33 (**8**): 086803. DOI: 10.1088/1674-1056/ad51f4

Controlled fabrication of freestanding monolayer SiC by electron irradiation

Yunli Da(笪蕴力), Ruichun Luo(罗瑞春), Bao Lei(雷宝), Wei Ji(季威), and Wu Zhou(周武)
Chin. Phys. B, 2024, 33 (**8**): 086802. DOI: 10.1088/1674-1056/ad6132

SPECIAL TOPIC — Stephen J. Pennycook: A research life in atomic-resolution STEM and EELS

Real-time four-dimensional scanning transmission electron microscopy through sparse sampling

A W Robinson[1,†], J Wells[1], A Moshtaghpour[3], D Nicholls[1], C Huang[3], A Velazco-Torrejon[3], G Nicotra[4], A I Kirkland[3], and N D Browning[1,6]

[1] *SenseAI Innovations Ltd., Liverpool, UK*
[2] *Centre for Doctoral Training, University of Liverpool, Liverpool, UK*
[3] *Correlative Imaging Group, Rosalind Franklin Institute, Oxford, UK*
[4] *CNR-IMM, Z.I. VIII Strada* 5, *Catania*, 95121, *Italy*
[5] *Department of Mechanical, Materials, and Aerospace Engineering, University of Liverpool, Liverpool, UK*

(Received 23 August 2024; revised manuscript received 16 October 2024; accepted manuscript online 23 October 2024)

Four-dimensional scanning transmission electron microscopy (4-D STEM) is a state-of-the-art image acquisition mode used to reveal high and low mass elements at atomic resolution. The acquisition of the electron momenta at each real space probe location allows for various analyses to be performed from a single dataset, including virtual imaging, electric field analysis, as well as analytical or iterative extraction of the object induced phase shift. However, the limiting factor in 4-D STEM is the speed of acquisition which is bottlenecked by the read-out speed of the camera, which must capture a convergent beam electron diffraction (CBED) pattern at each probe position in the scan. Recent developments in sparse sampling and image inpainting (a branch of compressive sensing) for STEM have allowed for real-time recovery of sparsely acquired data from fixed monolithic detectors, Further developments in compressive sensing for 4-D STEM have also demonstrated that acquisition speeds can be increased, i.e., live video rate 4-D imaging is now possible. In this work, we demonstrate the first practical implementations of compressive 4-D STEM for real-time inference on two different scanning transmission electron microscopes.

Keywords: compressive sensing, 4-D STEM, inpainting

PACS: 68.37.Ma, 61.72.uf, 07.05.Pj, 07.05.Hd **DOI:** 10.1088/1674-1056/ad8a4a

1. Introduction

The scanning transmission electron microscope (STEM) is the state-of-the-art machine for imaging atomic-scale structures. Over the past three decades, the field has been revolutionized by the development of aberration correctors,[1,2] brighter and more coherent electron sources, as well as improvements to electron detectors[3–7] and spectrometers. As a result, it is now possible to directly image complex samples, such as quantum materials,[8] two-dimensional materials,[9,10] metal–organic frameworks,[11,12] and interfaces between semiconducting materials.[13–16] The use of *Z*-contrast STEM, pioneered by Stepehen J. Pennycook, has enabled extensive atomic-scale characterization of these complex samples by collecting the intensity of the high-angle scattering signal which is proportional to the atomic number of the atom being imaged.[17,18] Furthermore, the inclusion of bright field imaging,[19] electron energy loss spectroscopy (EELS)[20], energy dispersive x-ray spectroscopy (EDS),[21] and four-dimensional STEM (4-D STEM)[22–24] has allowed further correlative chemical, electrical and structural characterization.

To acquire a 4-D STEM dataset, a convergent beam electron diffraction (CBED) pattern is captured in the far-field by a 2-D detector at each desired probe location on the sample plane as depicted in Fig. 1. This means, for each value in the dataset, it is given by both a scattering vector and a position vector. This allows the electron momenta to be resolved, as opposed to a single integration for each probe position as in a fixed monolithic radial detector. Modern direct electron detectors are typically capable of operating at speeds on the order of 10 kHz, with some being able to operate on the order of 100 kHz with limited bit-depth and read-out dimensions. This implies that a 4-D STEM dataset can be reasonably acquired with a dwell-time of 10 µs–100 µs. Work by O'Leary *et al.*[25] showed that 4-D STEM analysis can be applied to single bit-depth CBED patterns, increasing the frame rate whilst reducing the likelihood of sample drift and lens instabilities. However, as raised within this work, the detector becomes saturated if the probe current is too high. It is therefore preferable to retain a high dynamic range on the detector whilst also increasing the effective frame rate by other means.

An alternative method is to use the IDES Relativity™ system to increase the effective frame rate. Here, a deflector module is installed above the detector to rapidly shift the projected beam onto a new subregion of the detector. This allows for multiple CBED patterns to be read out within one read-out

[†]Corresponding author. E-mail: alex.robinson@senseai.vision

© 2024 Chinese Physical Society and IOP Publishing Ltd

instance (i.e., the acquisition of a total frame). This method can allow up to 300 kHz read-out speed if the detector itself is not limiting the total read-out of all subframes within one total frame.[26]

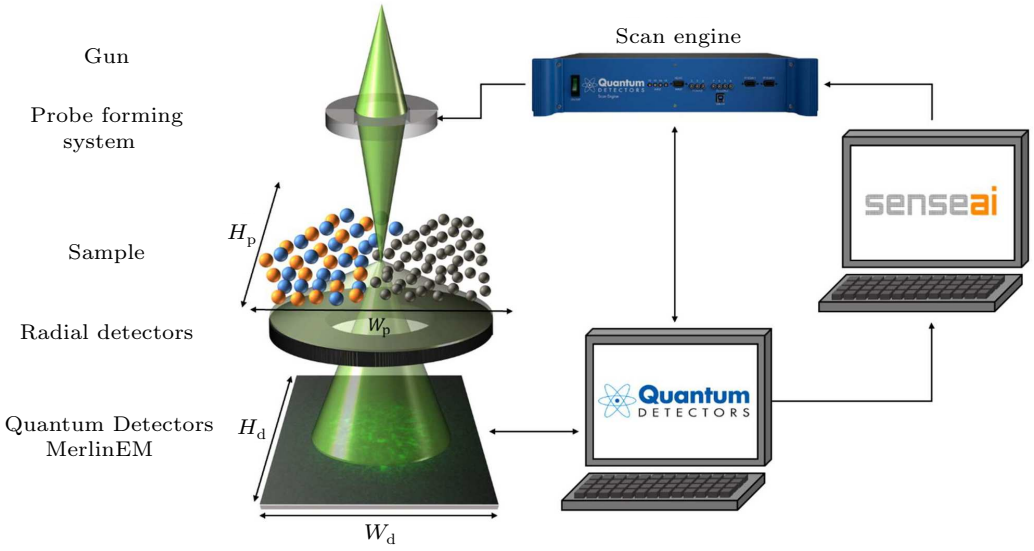


Fig. 1. Schematic showing the experimental set-up for acquiring a sub-sampled 4-D STEM dataset. The SenseAI PC (right) informs the scan engine (top middle) to position the probe at a given location for a given dwell time. The scan engine also informs the QD MerlinEM PC (bottom middle) of how long to acquire the frame on the detector. Once the frame has been acquired, it is sent via TCP to the SenseAI PC where it is processed. The detector height and width are given as H_d and W_d, respectively, and the scan height and width are given as H_p and W_p, respectively.

Another solution is to use compressive sensing, or specifically probe sub-sampling, where only a random subset of probe locations is acquired over the typical raster grid. Compressive sensing for electron microscopy has been demonstrated in many different imaging modalities, such as in Z-contrast STEM,[27] cryogenic FIB-SEM,[28] STEM simulations,[29,30] and more recently has been demonstrated to allow for significant decrease in the data acquisition requirement of 4-D STEM for focused probe acquisitions.[31] By leveraging the inherent sparsity within the real space domain, dictionary learning/sparse coding can faithfully inpaint the missing pixel data for each virtual image.

In this work, we demonstrate the practical implementation of compressive 4-D STEM to allow for live alignment using virtual images reconstructed from sub-sampled data. We demonstrate this method implemented on two independent machines, and that it is possible to achieve real-time 4-D STEM at traditional scanning dimensions.

2. Methods

We begin by presenting our data acquisition model based on that described in Ref. [31]. Assume a regular real space grid with a height and width of H_p, $W_p \in N$ respectively containing $\Omega_p := \{1,\ldots,H_p\} \times \{1,\ldots,W_p\}$ possible probe locations, and a 2-dimensional detector positioned in the far-field with a height and width (in pixels) of $H_d, W_d \in N$ respectively. The maximum number of CBED patterns that can be acquired is $N_p = H_p W_p$. The scan-step (scan-pitch) defined by the real space grid is given as $\Delta_p \in R^+$ measured in Ångstroms (Å), and the reciprocal space sampling on the detector is given as $\Delta_d \in R^+$ measured in milliradians (mrad). A real space vector corresponding to a given probe location is given as $\boldsymbol{r}_p \in R^2$, and a reciprocal space vector is given as $\boldsymbol{k}_d \in R^2$. The 4-D STEM dataset is then given as $\chi(\boldsymbol{r}_p, \boldsymbol{k}_d) \in R$, where each discrete element of the 4-D data is a real valued intensity. A CBED pattern is therefore $\boldsymbol{D}_{\boldsymbol{r}_p} := \chi(\boldsymbol{r}_p, \cdot) \in R^{H_d \times W_d}$, and a virtual image is therefore $\boldsymbol{X}_{\boldsymbol{k}_d} := \chi(\cdot, \boldsymbol{k}_d) \in R^{H_p \times W_p}$.

We determine a sampling mask based on a method known as lane-constrained sampling, which is a rasterized uniform density sampling (UDS) where each subsequent random pixel selection is in a rastered order (i.e., from left to right). Unlike using a beam blanker, the beam moves directly from one probe location to the next desired probe location regardless of the distance between them. Lane-constrained sampling is designed to minimize the unwanted effects of scan coil hysteresis as a result of non-rigid scanning patterns whilst retaining a UDS mask. This mask contains $M_p \ll N_p$ measurements (or probe locations) in the subsampling set $\Omega \subset \Omega_p$. Each measured virtual image is therefore

$$\boldsymbol{Y}_{\boldsymbol{\kappa}} = \boldsymbol{P}_{\Omega}(\boldsymbol{X}_{\boldsymbol{\kappa}}) + \boldsymbol{N}_{\boldsymbol{\kappa}} \in \boldsymbol{R}^{H_p \times W_p}$$

for each $\boldsymbol{\kappa} \in \boldsymbol{k}_d$. $\boldsymbol{P}_{\Omega}$ is a mask operator where $(\boldsymbol{P}_{\Omega}(\boldsymbol{U}))_{(i,j)} = \boldsymbol{U}_{(i,j)}$ if $(i,j) \in \Omega$ and $(\boldsymbol{P}_{\Omega}(\boldsymbol{U}))_{(i,j)} = 0$ otherwise, and $\boldsymbol{N}_{\boldsymbol{k}_d}$ is an additive noise. We now wish to form a virtual detector (VD) to apply to the acquired CBED patterns to form a virtual detector image (VDI). Firstly, we define the inner and outer collection semi-angles for each detector we require. We then integrate the signal which is generated by taking the Hadamard

product of the defined virtual detector with each of the CBED patterns (i.e., by summing the signal constrained by the VD). This integrated signal is then assigned to the specific probe location corresponding to each of the CBED patterns. Extended details on VDI formation can be found in the supplemental material of Ref. [31]. VDI examples can be seen in Fig. 2, along with the corresponding VD and sampling mask.

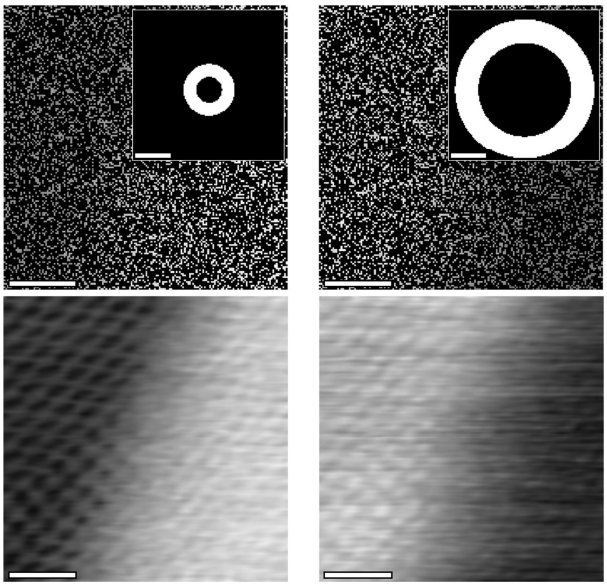


Fig. 2. Virtual annular bright field sub-sampled image (top left) and virtual low-angle dark field image (top right) taken from a sub-sampled 4-D STEM dataset. We can use inpainting to recover the virtual detector images (bottom row). The scale-bar for the virtual detector images corresponds to 1 nm, and the scale-bar for the virtual detectors corresponds to 30 mrad. Data acquired at the CNR-IMM, Catania, Italy. The CdTe/Si sample provided by Sivananthan Laboratories, IL, USA.

To perform real-time VDI formation, we use the Beta-Process Factor Analysis algorithm to inpaint the sub-sampled virtual detector images. Our implementation of this algorithm is implemented in C++ using CUDA for GPU acceleration. A mathematical description of the algorithm can be found in Refs. [32,33]. In principle, however, the sub-sampled image is broken down into a series of overlapping patches, which each act as independent training elements for a global dictionary. A dictionary is a high-level representation of the data that represents basis signals which can be linearly combined to form approximations of the target signal at each overlapping patch. When the overlapping patches are recombined, they form an approximation of the target signal across the entire image. The BPFA is an iterative process which is expected to converge towards a static set of dictionary elements and sparse weights.

In order to practically acquire the sub-sampled 4-D STEM data, we use a Quantum Detectors MerlinEM detector and a Quantum Detectors scan engine. The scan engine allows us to move the beam to any position on the sample without any need to blank the beam and therefore reduces the scan time. Both the detector and the scan engine are directly controlled by our software (SenseAI), allowing us to both control the beam position and record frames simultaneously, with a schematic given in Fig. 1. To automate as much of the data processing as possible, we implement automatic calibration of the CBED center and radius (in pixels). This is done by masking the average CBED after a fixed number of CBEDs have been acquired, by setting a threshold as a function of the maximum intensity of the average CBED. Any intensities below that threshold within the CBED are set to zero, and any greater or equal to that threshold are set to one. We then calculate the center of mass for that CBED to determine the center, then we apply a Sobel kernel to the mask to find the edge of the average CBED, which we can then use to determine the radius of the CBED. By knowing the convergence semi-angle, we can estimate Δ_{k} directly. In future applications, we intend to calibrate the reciprocal sampling by using a vacuum probe initially and then periodically updating the calibration as described.

At the beginning of an acquisition, we include our required VDs and set the collection semi-angles. In the case of annular bright field (ABF), we chose to collect signals between 11 mrad and 22 mrad (using a 30 mrad convergence semi-angle) and in the case of low angle annular dark field (LAADF), we chose to collect signals between 30 mrad and 60 mrad. Although not demonstrated here, we can also permit any arbitrary VD, as well as live center of mass and differential phase contrast.

3. Results

We now present the results of live sub-sampled 4-D STEM by looking at two different samples on two different microscopes. In all cases, we acquire and present only the results from the subsampled experiments and validation of the integrity of our inpainting methods can be found in Refs. [27–29,31]. The first is a gold polycrystal which is deposited on top of a germanium substrate, acquired using a JEOL GrandARM 2 at the Rosalind Franklin Institute. The data was acquired using a Quantum Detectors MerlinEM camera operating at a 12-bit depth with parameters $H_{\mathrm{d}} = W_{\mathrm{d}} = H_{\mathrm{p}} = W_{\mathrm{p}} = 256$, $M = 16384$ (i.e., 25% sampling), and $\Delta_{\mathrm{p}} \geq 0.05$ nm, and a probe current of approximately 60 pA. The camera read-out speed was therefore approximately 1200 fps, with an effective readout speed of 4800 fps. The bandwidth limited spatial sampling based on the 30.8 mrad convergence semi-angle and 300 kV accelerating voltage was 0.016 nm. We acquired the LAADF signal using inner and outer collection semi-angles of 30 mrad and 60 mrad, respectively. Still frames from the live capture of the data are shown in Fig. 3.

Although from a materials science perspective, this result may be trivial given that it is a standard sample, we have shown that an aperiodic structure (a polycrystal) can be inpainted in real time using a sparsely sampled 4-D STEM dataset. During the scan, the field of view was changed using the stage

controller and magnification. The smaller nanoparticle (left side of the left most frame in Fig. 3) was then moved out of the field of view to demonstrate that the inpainting algorithm can adapt to these changes in real-time. We also verified that alignment could be performed using the LAADF image by adjusting the stigmators and defocus values directly on the microscope. This can be seen in the change from frame (b) to (a) in Fig. 3 as the zoomed region has a visual improvement to the astigmatic aberration. We also see that the image artefacts which are typical due to stage movement are preserved in Figs. 3(a) and 3(b), showing that the same adjustments can be made in both an inpainted and fully sampled image. We refer readers to Ref. [34] for a video feed showing these adjustments in real time.

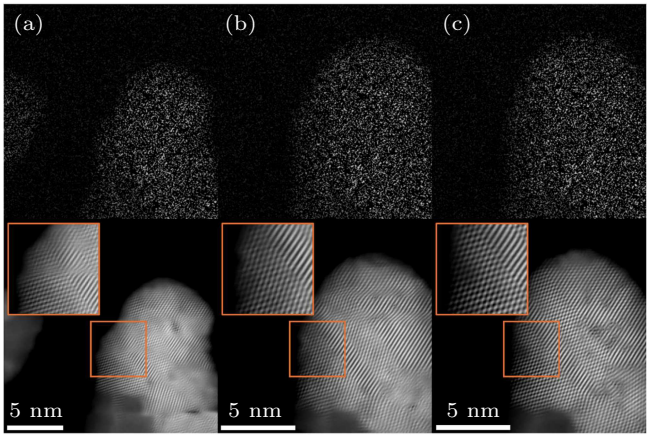


Fig. 3. Live capture and inpainting of sub-sampled 4-D STEM data of a gold nanoparticle on a germanium substrate. The top row is the acquired VDI, and the bottom row is the inpainted VDI with an overlay of a specific region. The frames are taken from the video feed at approximately 10 s (a), 20 s (b), and 30 s (c). As can be seen, the field of view, magnification, defocus and astigmatism can be amended using the virtual LAADF reconstruction. As the acquisition progresses from panel (a) to panel (c), the stage position is being adjusted and the field of view is changing to allow for the final image formed in panel (c). This demonstrates that the VDI is being used directly to improve the final 4-D STEM result. Data acquired at the Rosalind Franklin Institute, Oxford, UK. Sample provided by the Rosalind Franklin Institute, Oxford, UK.

We then performed a similar experiment at the National Research Council of Italy – Institute for Microelectronics and Microsystems (CNR-IMM) in Catania. This time we captured sub-sampled 4-D STEM measurements at the interface between silicon and germanium telluride. The data was acquired using a JEOL JEM-ARM 200F equipped with a Quantum Detectors MerlinEM camera operating at a 12-bit depth with parameters $H_\mathrm{d} = W_\mathrm{d} = 256$, $H_\mathrm{p} = W_\mathrm{p} = 512$, $M = 26214$ (i.e., 10% sampling), $\Delta_\mathrm{p} \geq 0.007$ nm, and a probe current of approximately 50 pA. The camera read-out speed was therefore approximately 1200 fps, with an effective readout speed of 12000 fps. The bandwidth limited spatial sampling based on the 30.0 mrad convergence semi-angle and 200 kV accelerating voltage was 0.021 nm. We acquired the LAADF signal using inner and outer collection semi-angles of 30 mrad and 60 mrad, respectively, and the ABF signal using inner and outer collection semi-angles of 11 mrad and 22 mrad respectively. Still frames from the live capture of the data are shown in Fig. 4.

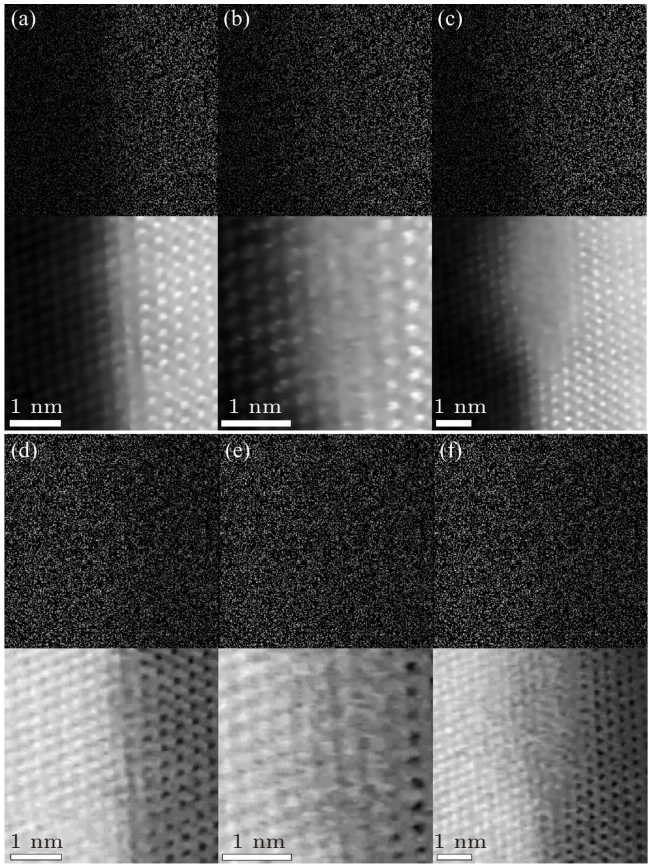


Fig. 4. Live capture and inpainting of sub-sampled 4-D STEM data of an interface between silicon and germanium telluride. In this live acquisition, we simultaneously image the LAADF (a)–(c) and ABF (d)–(e) signals and inpaint them on-the-fly. We start with a pristine boundary [(a) and (d)] acquired at 200 s after finding the region and correcting low-order aberrations, then increase the magnification to induce beam damage at the interface [(b) and (e)]. This causes the interface to breakdown and for tellurium to diffuse across the boundary. The final damaged section can be seen after demagnifying [(c) and (f)]. Data acquired at CNR-IMM, Catania, Italy. Sample provided by CNR-IMM, Catania, Italy.

As can be seen in Fig. 4, as the boundary is continually exposed, the sample is beginning to damage. We believe that tellurium atoms can be seen to diffuse across the boundary and either occupy silicon sites within the silicon lattice or occupy interstitial sites. In the final frame, the damaged region can be distinctly recognized in the pristine sample. By deliberately damaging the sample, it allowed us to visualize the damage mechanism and resulting dynamics within a 4-D STEM framework, even using a 2-D detector running at modest speeds. If we also chose to reduce the read-out area of the detector, and to decrease the bit depth, we would expect that the Quantum Detectors MerlinEM incorporating sparse sampling could have read a 512×512 scanning region in less than one second (assuming a camera readout speed of 2 kHz at 12-bit for a single chip, the expected speed up is $8\times$ for reducing the read-out to a 32×256 readout region, and $2\times$ for 6-bit. Including

sparse sampling at 10% increases the effective read-out speed by 10×. This gives an effective readout speed of 320 kHz).

4. Conclusion

The results of this work demonstrate that a live 4-D STEM experiment can be performed using sparse sampling techniques. Given the modularity of the approach, the increase in speed can be extrapolated to any existing 2-D detector, including those running at the highest frame rates available. Not only does sparse sampling offer an increase in speed for small fields on view, it can also offer a solution for improved stability over large scanning region, reducing drift artefacts and data storage requirements. The results show that potentially the effective frame rate of any camera can be improved using image inpainting. By acquiring fewer data points over the same field of view, the speed of acquisition increases.

Our future work will focus on *in-situ* 4-D STEM, with the goal of imaging dynamical processes within complex materials such as battery cathodes and perovskites. Using these techniques, we expect that the limiting factor for 4-D STEM is no longer the speed of acquisition, but the stability of the sample, the scanning coils, and lens systems.

Acknowledgments

The authors would like to thank the Rosalind Franklin Institute for providing access to the JEOL GrandARM 2 “Ruska” and National Research Council of Italy’s Institute for Microelectronics and Microsystems at Catania for providing access to the JEOL JEM-ARM 200F to gather results for this work. We thank the Royal Society for providing funding under grant number EGR10965. A.W.R., D.N., J.W., and N.D.B. are cofounders of SenseAI Innovations Ltd. which provides the software to reconstruct the data presented.

References

[1] Krivanek O L, Dellby N and Lupini A R 1999 *Ultramicroscopy* **78** 1
[2] Batson P E, Dellby N and Krivanek O L 2002 *Nature* **418** 617
[3] Faruqi A R and McMullan G 2018 *Nucl. Instrum. Methods Phys. Res. A* **878** 180
[4] Faruqi A R, Henderson R, Pryddetch M, Allport P and Evans A 2005 *Nucl. Instrum. Methods Phys. Res. A* **546** 170
[5] Ciston J, Johnson I J, Draney B R, Ercius P, Fong E, Goldschmidt A, Joseph J M, Lee J R, Mueller A, Ophus C, Selvarajan A, Skinner D E, Stezelberger T, Tindall C S, Minor A M and Denes P 2019 *Microscopy and Microanalysis* **25** 1930
[6] Ryll H, Simson M, Hartmann R, Holl P, Huth M, Ihle S, Kondo Y, Kotula P, Liebel A, Müller-Caspary K, Rosenauer A, Sagawa R, Schmidt J, Soltau H and Strüder L 2016 *J. Instrument.* **11** P04006
[7] Yang H, Jones L, Ryll H, Simson M, Soltau H, Kondo Y, Sagawa R, Banba H, MacLaren I and Nellist P D 2015 *J. Phys. Conf. Ser.* **644** 012032
[8] Zheng Q, Feng T, Hachtel J A, Ishikawa R, Cheng Y, Daemen L, Xing J, Idrobo J C, Yan J, Shibata N, Ikuhara Y, Sales B C, Pantelides S T and Chi M 2021 *Sci. Adv.* **7** eabe6819
[9] Mas-Ballesté R, Gómez-Navarro C, Gómez-Herrero J and Zamora F 2011 *Nanoscale* **3** 20
[10] Novoselov K S, Mishchenko A, Carvalho A and Castro Neto A H 2016 *Science* **353**
[11] Mayoral A, Mahugo R, SánchezSánchez M and Díaz I 2017 *ChemCatChem* **9** 3497
[12] Shen B, Chen X, Shen K, Xiong H and Wei F 2020 *Nat. Commun.* **11** 2692
[13] Pennycook S J, McGibbon A J, McGibbon M M, Browning N D, Chisholm M F and Jesson D E 1994 *Determination of interface structure and bonding at atomic resolution in the STEM*, in *Proceedings of the 13th International Congress on Electron Microscopy*, Paris (France), 17-22 July, 1994
[14] Benthem K and Pennycook S J 2009 *Appl. Phys. A* **96** 161
[15] Chisholm M F and Pennycook S J 2006 *Philosoph. Mag.* **86** 4699
[16] Chejarla V S, Ahmed S, Belz J, Scheunert J, Beyer A and Volz K 2023 *Small Methods* **7**
[17] Pennycook S J, Rafferty B and Nellist P D 2000 *Microscopy and Microanalysis* **6** 343
[18] Pennycook S J and Jesson D E 1991 *Ultramicroscopy* **37** 14
[19] Kim Y M, Pennycook S J and Borisevich A Y 2017 *Ultramicroscopy* **181** 1
[20] Egerton R F 2011 *Electron energy-loss spectroscopy in the electron microscope* (Springer Science & Business Media)
[21] Chang T Y, Tanaka Y, Ishikawa R, Toyoura K, Matsunaga K, Ikuhara Y and Shibata N 2014 *Nano Lett.* **14** 134
[22] Ophus C 2019 *Microscopy and Microanalysis* **25** 563
[23] Bustillo K C, Zeltmann S E, Chen M, Donohue J, Ciston J, Ophus C and Minor A M 2021 *Acc. Chem. Res.* **54** 2543
[24] Wen Y, Ophus C, Allen C S, Fang S, Chen J, Kaxiras E, Kirkland A I and Warner J H 2019 *Nano Lett.* **19** 6482
[25] O’Leary C M, Allen C S, Huang C, Kim J S, Liberti E, Nellist P D and Kirkland A I 2020 *Appl. Phys. Lett.* **116** 124101
[26] Tan J A, Dull J T, Zeltmann S E, Tulyagankhodjaev J A, Johnson H M, LiebmanPeláez A, Folie B D, Dönges S A, Khatib O, Raybin J G, Roberts T D, Hamerlynck L M, Tanner C P N, Lee J, Ophus C, Bustillo K C, Raschke M B, Ohldag H, Minor A M, Rand B P and Ginsberg N S 2023 *Adv. Funct. Mater.* **33**
[27] Nicholls D, Robinson A, Wells J, Moshtaghpour A, Bahri M, Kirkland A and Browning N 2022 *Proceedings of the IEEE International Conference on Acoustics, Speech and Signal Processing (ICASSP)* pp. 1586–90
[28] Nicholls D, Wells J, Robinson A W, Moshtaghpour A, Kobylynska M, Fleck R A, Kirkland A I and Browning N D 2022 arXiv: 2211.03494
[29] Robinson A W, Wells J, Nicholls D, Moshtaghpour A, Chi M, Kirkland A I and Browning N D 2023 *J. Microsc.* **290** 53
[30] Robinson A, Nicholls D, Wells J, Moshtaghpour A, Kirkland A and Browning N D 2022 *Ultramicroscopy* **242** 113625
[31] Robinson A W, Moshtaghpour A, Wells J, Nicholls D, Chi M, MacLaren I, Kirkland A I and Browning N D 2024 *J. Microsc.* **295** 278
[32] Sertoglu S and Paisley J 2015 2015 23*rd European Signal Processing Conference (EUSIPCO)* p. 2771
[33] Zhou M, Chen H, Paisley J W, Ren L, Sapiro G and Carin L 2009 *NIPS* **9** 2295
[34] SenseAI Innovations Ltd. Live Subsampled 4D-STEM with SenseAI